Electronic Supplementary Material (ESI) for Materials Advances.
This journal is © The Royal Society of Chemistry 2023

Electronic Supplementary Information

Aerosol-Assisted Chemical Vapour Deposition of Highly Efficient Mixed Anatase-Rutile TiO2 for Photoelectrochemical Water Splitting

Thom R. Harris-Lee,[ab] Enrico Della Gaspera,[c] Frank Marken,[a] Jie Zhang,[b] Cameron L. Bentley[b] and Andrew L. Johnson*[a]

[a] *Department of Chemistry, University of Bath, Claverton Down, Bath, BA2 7AY, UK*

[b] *School of Chemistry, Monash University, Clayton, Vic 3800, Australia*

[c] *School of Science, RMIT University, Melbourne, VIC, 3000, Australia*

S1. Sample Notation

Table S1. All AACVD conditions used for each sample, along with the notation used in main text according to the specified system. The samples using 'standard deposition procedure' for each precursor are highlighted in green.

Sample Notation	Precursor	Deposition Temperature / °C	Deposition Time / min	Precursor Concentration / mmol dm^{-3}
TiO_2-3	3	450	120	100
TiO_2-3-80mM	3	450	120	80
TiO_2-3-120mM	3	450	120	120
TiO_2-3-60min	3	450	60	100
TiO_2-3-90min	3	450	90	100
TiO_2-3-500°C	3	500	120	100
TiO_2-4	4	450	120	100
TiO_2-4-80mM	4	450	120	80
TiO_2-4-120mM	4	450	120	120
TiO_2-4-60min	4	450	60	100
TiO_2-4-90min	4	450	90	100
TiO_2-4-500°C	4	500	120	100

S2. Experimental Methods

S2.1 Chemicals and Solvents

All starting chemicals were provided by Sigma Aldrich, Fisher Scientific, Alfa Aesar or Acros organics without further purification unless otherwise stated. All solvents, except Diethyl ether (Et_2O) and tetrahydrofuran (THF), were dried through anhydrous alumina columns using an Innovative Technology Inc. PS-400-7 solvent purification system. Solvents were then degassed using cold vacuum degassing at 77K, followed by argon dissolution back into the solvent at room temperature. Et_2O and THF were degassed twice by cold vacuum degassing, prior to being dried by reflux over potassium in the presence of benzophenone followed by isolation via vacuum distillation. All solvents were stored in J Youngs ampules over molecular sieves. Deuterated benzene (C_6D_6) NMR solvent was purchased from Sigma-Aldrich and dried by refluxing over potassium before isolation by vacuum distillation. Anhydrous deuterated chloroform ($CDCl_3$) was purchased from Sigma-Aldrich and used without further purification.

S2.2 General

All reactions were performed under inert conditions, standard Schlenk line and glove box techniques under an Argon atmosphere.

Electronic Supplementary Information

Nuclear magnetic resonance (NMR) experiments were conducted in J Young's tap NMR tubes, prepared and sealed in a glovebox. NMR spectra were collected at 25 °C and recorded on an Agilent-500 (^{1}H NMR at 500 MHz, ^{13}C{^{1}H} NMR at 126 MHz). Proton and carbon chemical shifts are reported in parts per million (ppm) downfield from tetramethylsilane and referenced to the residual protium and carbon resonances respectively in the solvent (benzene, C_6D_6) peaks (^{1}H NMR: C_6D_6 at 7.16 ppm, ^{13}C{^{1}H} NMR: C_6D_6 at 128.1 ppm. NMR data are written as follows: chemical shift, multiplicity, integration, species.

All crystallographic data was collected at 150(2) K on an Agilent Xcalibur or Agilent SuperNova, Dual, EosS2 diffractometer using radiation Cu-Kα (λ = 1.54184 Å) or Mo-Kα (λ = 0.71073 Å). All structures were solved by direct methods followed by full-matrix least squares refinement on F2 using the WINGX-2014 suite of programs[1] or OLEX2.[2] All hydrogen atoms were included in idealised positions and refined using the riding model. Crystals were isolated from an argon filled Schlenk flask and immersed under oil before being mounted onto the diffractometer. CSD 2260244-2260247 contains the supplementary crystallographic data for this paper. These data can be obtained free of charge at www.ccdc.cam.ac.uk/conts/retrieving.html or from the Cambridge Crystallographic Data Centre, 12, Union Road, Cambridge CB2 1EZ, UK; fax: +44-1223/336-033; E-mail: deposit@ccdc.cam.ac.uk.

Thermogravimetric analysis was performed air sensitively, using a PerkinElmer Inc. TGA 4000 quartz microbalance instrument residing inside a glovebox. The TGA furnace was heated between 50 and 520 °C, at a constant ramp rate of 5 °C min^{-1} under an argon flow of 20 mL min^{-1}. Samples of the compounds were prepared in the glovebox using pre-weighed aluminium pans. PYRIS Version 10.1 Instrument managing and analysis software was used to record and analyse the data.

S2.3 AACVD Deposition

Fluorine-doped tin oxide (FTO) coated glass substrates were ultrasonically cleaned using deionised water, isopropanol, and acetone, then dried under N_2 flow and further cleaned using a low pressure O2 plasma reactor for 10 minutes. All substrates were immediately placed within the quartz tube for deposition to prevent potential contamination and dust particulates collecting on the substrate surface.

Thin films were deposited using a hot wall furnace system combined with a TSI 3076 Constant Output Atomiser. Argon carrier gas flow was monitored via a bubbler and a Bronkhorst flow meter, set at a constant flow rate of 1.5 L min^{-1}. The precursor solution was prepared inside a glovebox under argon atmosphere inside the precursor pot, which was then sealed before removing from the box and attaching to the AACVD rig. Once mounted, with substrate inside the quartz tube, argon gas was flowed through the system, with the precursor pot closed off and isolated, for one hour to purge the oxygen and moisture present. During purging, the furnace was heated to the desired temperature and allowed to equilibrate. Once this time has been completed, both taps on the precursor pot were simultaneously opened causing the precursor to be injected into the system as a fine aerosol. After the target deposition time had been reached, the pot taps were closed, and the furnace turned off. The furnace was left to cool to room temperature before removal of the substrate.

S2.4 Thin Film Characterisation

Electrochemical data was recorded with an Autolab electrochemical workstation (PGSTAT100) connected to a three-electrode electrochemical cell containing a platinum wire counter electrode (CE), 3 M Ag/AgCl reference electrode (RE) and thin film sample working electrode (WE). Simulated sunlight was generated from a 300 W Xenon lamp (Microsolar300 Beijing Perfectlight Technology Co. Ltd., AM 1.5G, 100 mW cm^{-2}) was employed to give chopped light (5 seconds on, 5 seconds off) incident on the

WE to demonstrate photocurrents and dark background currents across a potential range scanned with scan rate 15 mV s^{-1}. All measurements performed in 1 M KOH (pH 13.7) electrolyte.

Morphologies of the electrodes were obtained by field emission scanning electron microscopy (FEGSEM, JEOL JSM-7001F), and elemental analysis was performed by energy dispersive X-ray spectroscopy (EDX, Oxford Instruments AZtec). Analysis of the TiO_2 phase was achieved by powder X-ray diffraction (P-XRD, STOE STADI P Bragg-Brentano geometry) and Raman spectroscopy (Renishaw inVia, λ = 532 nm). Absorption spectra were collected on a Cary 5000 UV-Vis-NIR spectrophotometer equipped with an integrating sphere and a centermount sample holder to account for scattering and reflection contribution.

S2.5 Chemical Syntheses

[N{CH_2Me_2COH}$_3$] (**1**)

1,2-Epoxy-2-methylpropane (8.945 mL, 99 mmol) and ammonia (15 mL of 2 M NH_3 in ethanol, 30 mmol) were syringed into a sealed vessel, stirred at room temperature for 24 hours and then heated at 50 ^{o}C for 4 days. The product was washed with DCM and dried in vacuo, followed by recrystallisation in DCM. The resulting crystals were then isolated, redissolved in DCM, dried over Na_2SO_4, filtered, and pumped down to dryness in vacuo, yielding a fine, white free flowing powder (3.59 g, 15.40 mmol, 51.3%). Product was stored in an inert, glovebox environment due to its high hygroscopicity.

^{1}H NMR (500 MHz, C_6D_6) δ 2.55 (s, 6H, $OCMe_2\mathit{CH_2}N$), 1.14 (s, 18H, $OC\mathit{Me_2}CH_2N$).

^{13}C{^{1}H} NMR (126 MHz, C_6D_6) δ 70.69 ($O\mathit{C}Me_2CH_2N$), 70.36 ($OCMe_2\mathit{CH_2}N$), 28.83 ($OC\mathit{Me_2}CH_2N$).

[(Me_2N)Ti{$OCMe_2CH_2$}$_3$N] (**2**)

Complex 2 was synthesised by the dropwise addition of **1** (0.700 g, 3 mmol) to Ti(NMe2)4 (0.673 g, 3 mmol) under vigorous stirring, both in anhydrous tetrahydrofuran (THF). After 30 minutes stirring, the THF was removed in vacuo followed by a hexane wash. Subsequent evaporation of the hexane resulted in an orange solid of **2**.

^{1}H NMR (500 MHz, C_6D_6) δ 3.43 (s, 6H, $N\mathit{Me_2}$), 2.62 (s, 6H, $OCMe_2\mathit{CH_2}N$), 1.27 (s, 18H, $OC\mathit{Me_2}CH_2N$).

^{13}C{^{1}H} NMR (126 MHz, C_6D_6) δ 81.10 ($O\mathit{C}Me_2CH_2N$), 73.61 ($OCMe_2\mathit{CH_2}N$), 45.54 ($N\mathit{Me_2}$), 30.79 ($OC\mathit{Me_2}CH_2N$).

[(EtO)Ti{$OCMe_2CH_2$}$_3$N] (**3**)

The amine group on 2 can be replaced by an ethoxide by the addition of anhydrous ethanol (0.184 g, 4 mmol) in slight excess to 2 (0.967 g, 3 mmol) in anhydrous hexane. After overnight stirring, the orange solution changed colour to pale yellow. Filtration followed by evaporation of the hexane *in vacuo* resulted in a pale yellow solid of [(EtO)Ti{$OCMe_2CH_2$}$_3$N] (0.842 g, 2.604 mmol, 86.8%).

^{1}H NMR (500 MHz, C_6D_6) δ 4.50 (q, *J* = 7.0 Hz, 2H, $O\mathit{CH_2}CH_3$), 2.69 (s, 6H, $OCMe_2\mathit{CH_2}N$), 1.37 (t, *J* = 7.0 Hz, 3H, $OCH_2\mathit{CH_3}$), 1.25 (s, 18H, $OC\mathit{Me_2}CH_2N$).

^{13}C{^{1}H} NMR (126 MHz, C_6D_6) δ 81.82 ($O\mathit{C}Me_2CH_2N$), 74.28 ($OCMe_2\mathit{CH_2}N$), 70.68 ($O\mathit{CH_2}CH_3$), 31.02 ($OC\mathit{Me_2}CH_2N$), 19.77 ($OCH_2\mathit{CH_3}$).

[(iPrO)Ti{$OCMe_2CH_2$}$_3$N] (**4**)

An isoproxide functionalised titanium precursor was synthesised in a similar method to Mun *et al.*.[3] An anhydrous THF solution of 1 (0.700 g, 3 mmol) was added dropwise to Ti(O-*i*-Pr)$_4$ (0.853 g, 3 mmol) in anhydrous THF, giving a colourless liquid. After 30 minutes stirring, the THF was removed *in vacuo* followed by a hexane wash. Subsequent evaporation of the hexane *in vacuo* resulted in a white solid of $[(\mathrm{O}\text{-}i\text{-}\mathrm{Pr})\mathrm{Ti}\{\mathrm{OCMe_2CH_2}\}_3\mathrm{N}]$.

^{1}H NMR (500 MHz, C_6D_6) δ 4.80 (hept, *J* = 6.1 Hz, 1H, $\mathrm{O}\mathit{C}\mathrm{Me_2}$), 2.69 (s, 6H, $\mathrm{OCMe_2}\mathit{CH_2}\mathrm{N}$), 1.42 (dd, *J* = 6.0, 0.9 Hz, 6H, $\mathrm{OC}\mathit{Me_2}$), 1.25 (s, 18H, $\mathrm{OC}\mathit{Me_2}\mathrm{CH_2N}$).

^{13}C{^{1}H} NMR (126 MHz, C_6D_6) δ 81.37 ($\mathrm{O}\mathit{C}\mathrm{Me_2CH_2N}$), 75.89 ($\mathrm{O}\mathit{C}\mathrm{Me_2}$), 73.85 ($\mathrm{OCMe_2}\mathit{CH_2}\mathrm{N}$), 30.64 ($\mathrm{OC}\mathit{Me_2}\mathrm{CH_2N}$), 26.08 ($\mathrm{OC}\mathit{Me_2}$).

$[(\mu\text{-O})\{\mathrm{Ti(OCMe_2CH_2)_3N}\}_2]$ (**5**)

A bridging oxygen species was synthesised by the dropwise addition of water (0.027 g, 1.5 mmol) to **2** (0.967 g, 3 mmol) in anhydrous hexane, which after overnight stirring changed colour from orange to white. Hexane evaporation *in vacuo* prior to THF addition, filtration and evaporation of THF *in vacuo* resulted in a white solid of $[(\mu\text{-O})\{\mathrm{Ti(OCMe_2CH_2)_3N}\}_2]$ (0.627 g, 1.10 mmol, 36.5%).

^{1}H NMR (500 MHz, C_6D_6) δ 2.61 (s, 12H, $\mathrm{OCMe_2}\mathit{CH_2}\mathrm{N}$), 1.17 (s, 36H, $\mathrm{OC}\mathit{Me_2}\mathrm{CH_2N}$).

^{13}C{^{1}H} NMR (126 MHz, C_6D_6) δ 82.19 ($\mathrm{O}\mathit{C}\mathrm{Me_2CH_2N}$), 74.19 ($\mathrm{OCMe_2}\mathit{CH_2}\mathrm{N}$), 30.84 ($\mathrm{OC}\mathit{Me_2}\mathrm{CH_2N}$).

S3. Thermogravimetric Analysis

Table S2. Thermogravimetric analysis mass loss event data for compounds **2**, **3**, **4** under inert glovebox atmosphere.

	Mass-loss Event 1				Mass-loss Event 2				
Compound	**Onset T / °C**	**Onset %wt**	**End T / °C**	**End %wt**	**Onset T / °C**	**Onset %wt**	**End T / °C**	**End %wt**	**Target %wt**
2	101	99.0	202	20.5	210	19.2	305	5.8	24.8
3	119	99.0	203	35.4	227	32.3	284	10.9	24.7
4	121	99.0	205	7.7	-	-	-	2.0	23.7

Thermogravimetric analysis of all 3 compounds was also carried out in an ambient atmosphere to study the air and moisture stability of each during heating processes (Figure S1). Compound **2** showed an initial increase in mass, indicating oxidation occurring, with a mass-loss event onset and completion shifted approx. 50 °C higher. Compound **3**, contained multiple slow mass-loss events, followed by a more rapid drop to reach similar residual %wt as in inert atmosphere, and at similar temperature. Compound **4** also showed a slow decrease in mass at the beginning, but it still contained a single, fast mass-loss event to reach a similar residual %wt as in inert atmosphere, and a slightly (approx. 20 °C) increased completion temperature.

Electronic Supplementary Information

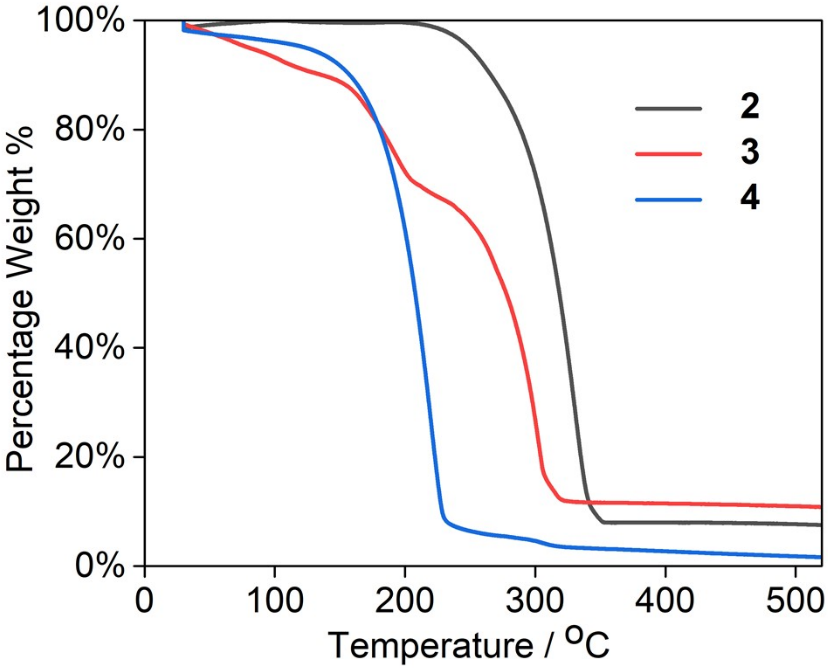

Figure S1. Thermogravimetric analysis of compounds **2**, **3**, **4**, measured under ambient atmospheric conditions between 30 and 520 °C at a constant ramp rate of 5 °C min^{-1}.

S4. Characterisation of TiO_2 Thin Films

S4.1 Scanning Electron Microscopy

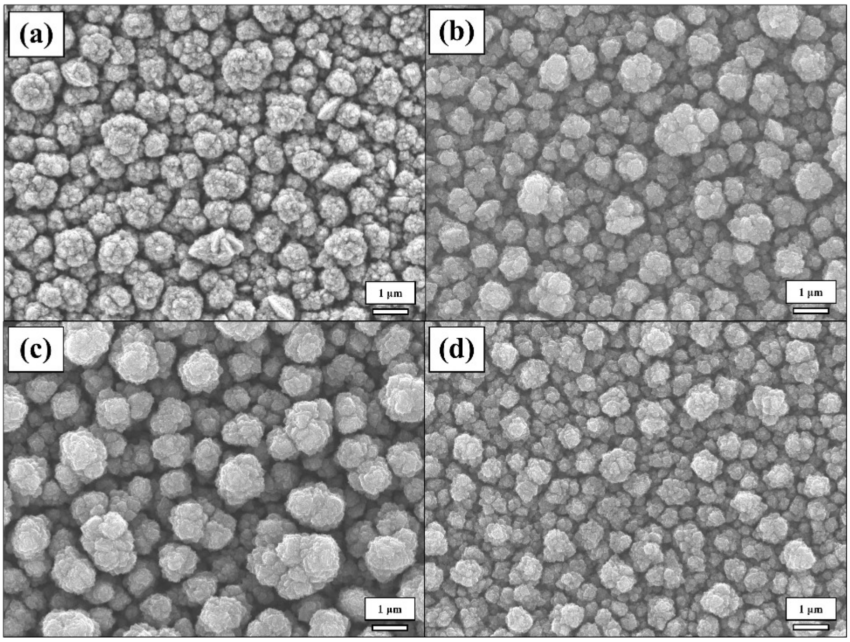

Figure S2. Top-down electron micrographs of (a) TiO_2-3, (b) TiO_2-3-80mM, (c) TiO_2-4, (d) TiO_2-4-80mM.

Due to the unusually high performance of pristine TiO_2 thin films reported here, energy dispersive X-ray spectroscopy (EDX) was undergone to confirm no accidental doping occurred during the deposition process. Resulting elemental maps from sample TiO_2-3 (Figure S3) clearly identified only Ti and O elements present from the film, with some Sn and Si from the FTO-coated glass substrate.

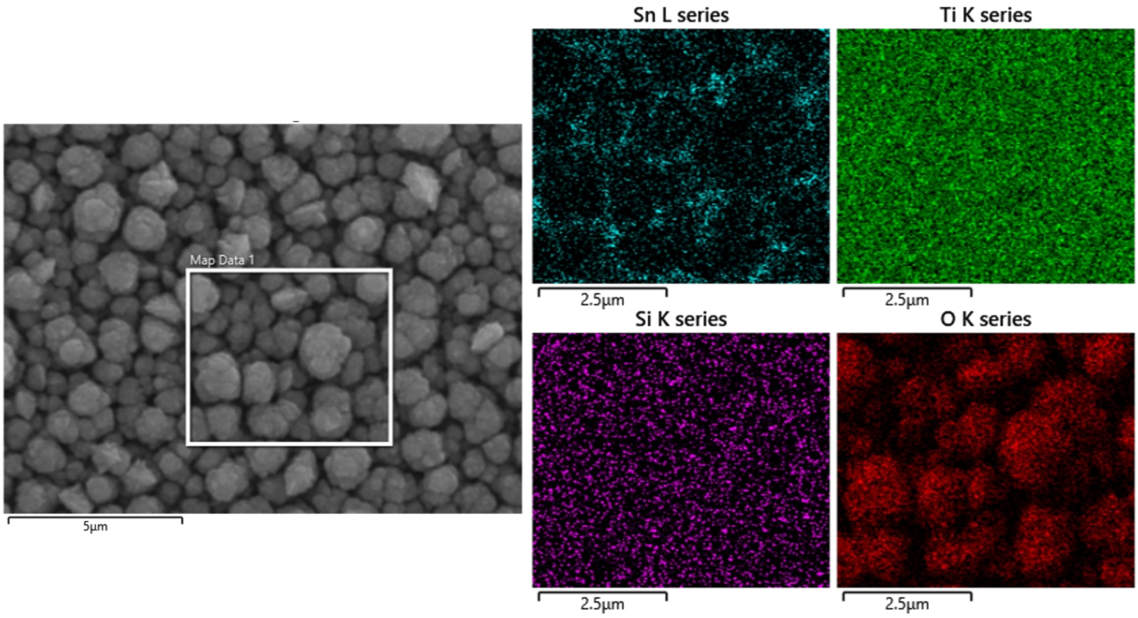

Figure S3. Energy dispersive X-ray spectroscopy (EDX) data for TiO_2-3.

S4.2 Grain Size and Phase Ratio Data

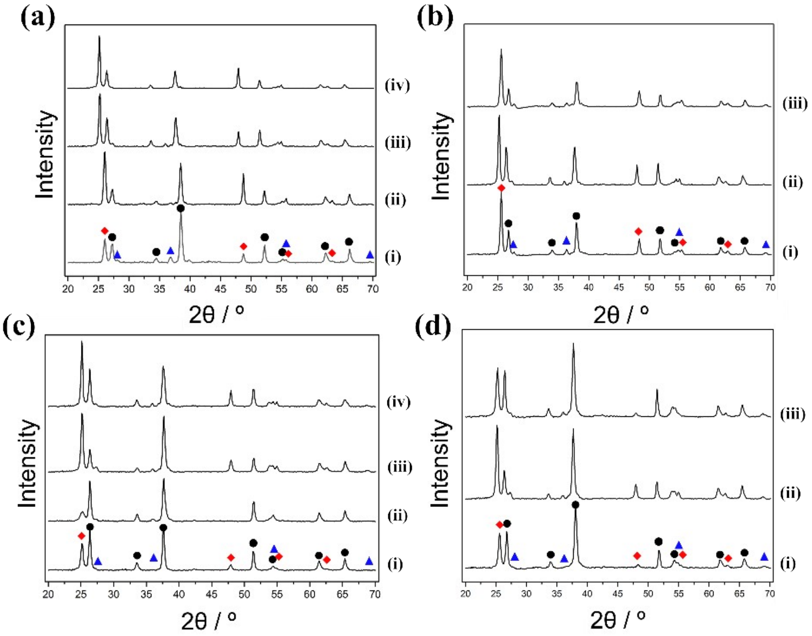

Figure S4. Reflection-XRD patterns for TiO_2 films obtained with (a) different deposition times (i) TiO_2-3-60min, (ii) TiO_2-3-90min, (iii) TiO_2-3, temperature (iv) TiO_2-3-500ºC; (b) (i) different precursor concentration TiO_2-3-80mM, (ii) TiO_2-3-100mM, (iii) TiO_2-3-120mM; (c) and (d) show the equivalent as (a) and (b) respectively, but with compound 4 as the precursor. On the first trace of each set, peaks corresponding to FTO are marked with a black dot, anatase with a red diamond, and rutile with a blue triangle.

Table S3. Complete phase fraction and grain size data. TiO_2-4-60min was not displayed in Figure 3 due to the lack of any visible deposit, and anomalous rutile grain size. Abbreviations: A = Anatase, R = Rutile.

Sample	%A	%R	A Grain Size / nm	R Grain Size / nm
TiO_2-3	95.6	4.4	29.3	27.4
TiO_2-3-80mM	93.3	6.7	23.4	26.6
TiO_2-3-120mM	94.2	5.8	21.8	26.2
TiO_2-3-60min	83.5	16.5	20.4	17.5
TiO_2-3-90min	97.2	2.8	21.9	18.0
TiO_2-3-500°C	99.3	0.7	27.6	22.1
TiO_2-4	96.1	3.9	23.3	13.7
TiO_2-4-80mM	96.9	3.1	20.4	11.6
TiO_2-4-120mM	91.3	8.7	19.2	25.4
TiO_2-4-60min	98.6	1.4	22.2	79.9
TiO_2-4-90min	87.9	12.1	11.2	16.8
TiO_2-4-500°C	95.9	4.1	27.8	29.0

S4.3 Raman Spectroscopy

Raman spectroscopy was carried out on TiO_2 films deposited by both precursors using varying precursors concentration (Figure S5). The spectra for all samples show dominantly anatase phase, with peaks labelled A1, A2, A3, A4, and A5 corresponding to modes E_g, E_g, B_{1g}, A_{1g}, and E_g respectively. On some of the spectra, a rutile phase peak can be seen (R1) corresponding to E_g mode, and evidence that there is rutile presence, albeit at very low relative intensity. Additionally, unseen B_{1g} and A_{1g} rutile peaks could some overlap with A1 and A5 respectively, therefore they are likely hidden by the overwhelming relative sizes of anatase contribution.

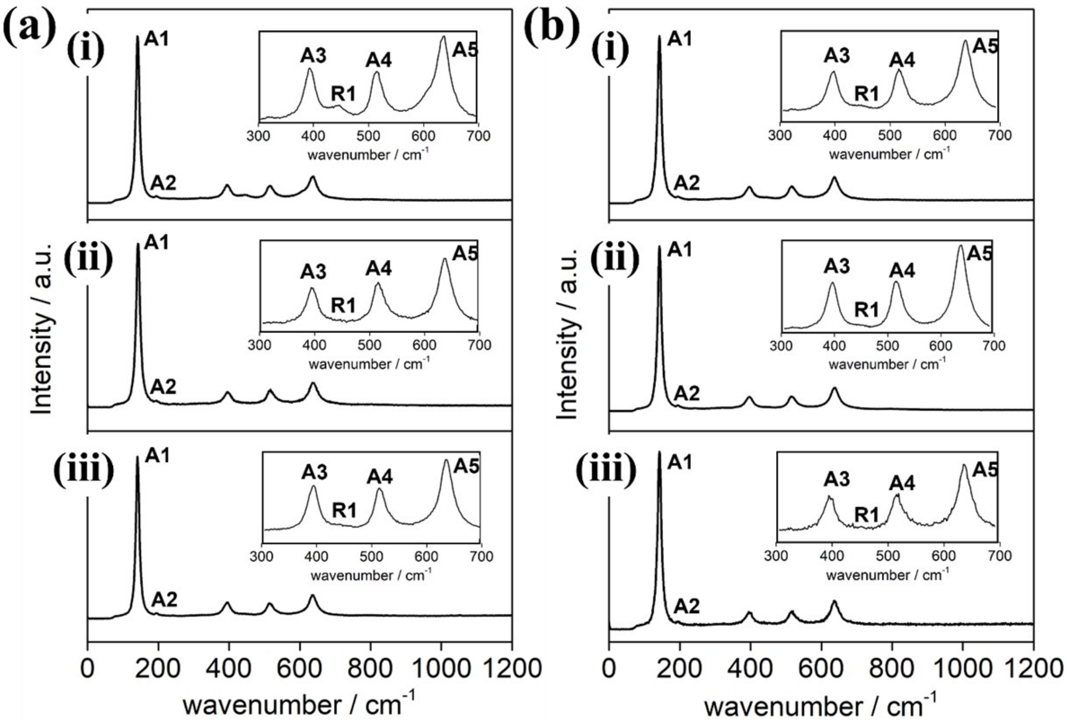

Figure S5. Raman spectra ($\lambda_{excitation}$ = 532 nm) for (a) (i) TiO2-3-120mM, (ii) TiO_2-3, (iii) TiO_2-3-80mM, (b) (i) TiO2-4-120mM, (ii) TiO_2-4, (iii) TiO_2-4-80mM. Anatase peaks are labelled as 'A' and rutile as 'R'. Inserts show a zoomed in view of the range 300-700 cm^{-1}.

S4.4 Absorption Spectroscopy and Band Gaps

Both TiO_2-3-80mM and TiO_2-4 show a sharp absorption onset at 405 nm (Figure S6), resulting in a band gap of ~3.08 eV, close to both anatase (~3.2 eV) and rutile (~3.0 eV), and consistent with both phases being present in the films. Given how close anatase and rutile band gaps are to one another, it is not expected to see two distinct transitions here.

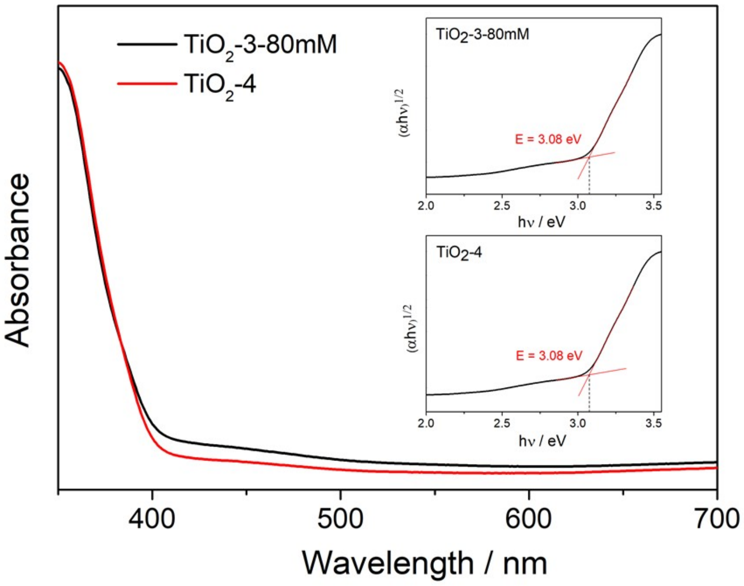

Figure S6. Optical absorption spectra for TiO_2-3-80mM (black) and TiO_2-4 (red), insets show Tauc plots for each electrode, as labelled.

S5. Photoelectrochemical Characterisation

S5.1 Rear-side Illumination

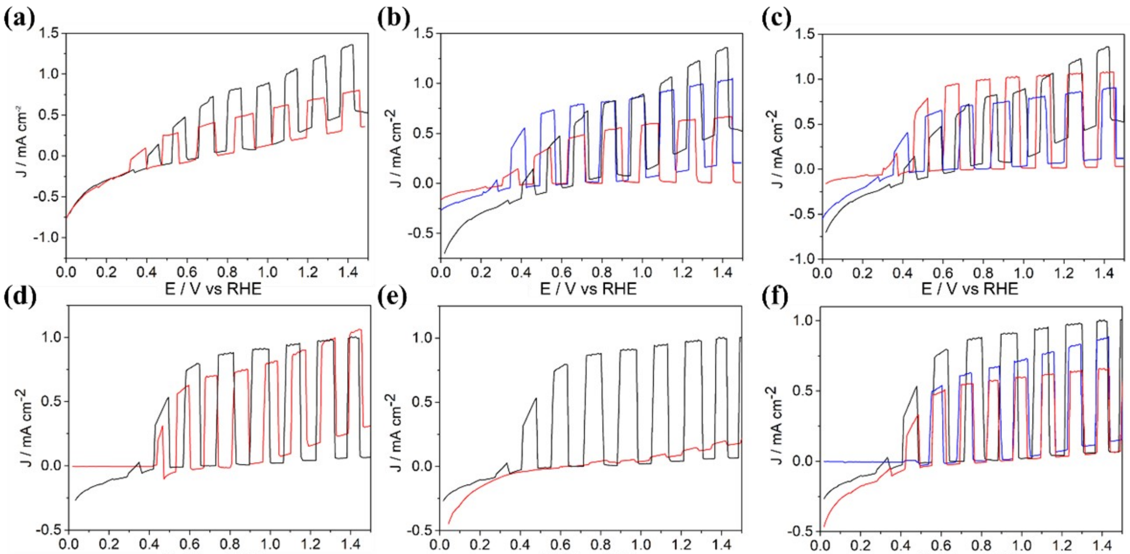

Figure S7. (a-f) Linear sweep voltammograms of TiO_2 thin films under 1 sun chopped AM 1.5 rear illumination with deposition condition variations of (a) temperature: black = TiO_2-3, red = TiO_2-3-500°C, (b) deposition time: black = TiO_2-3, red = TiO_2-3-90min, blue = TiO_2-3-60min, (c) concentration: black = TiO_2-3, red = TiO_2-3-80mM, blue = TiO_2-3-120mM, (d) temperature: black = TiO_2-4, red = TiO_2-4-500°C, (e) deposition time: black = TiO_2-4, red = TiO_2-4-90min, (f) concentration: black = TiO_2-4, red = TiO_2-4-80mM, blue = TiO_2-4-120mM. All measurements performed in 1 M KOH (pH 13.7) with a 15 mV s^{-1} scan rate.

S5.2 Front-side Illumination

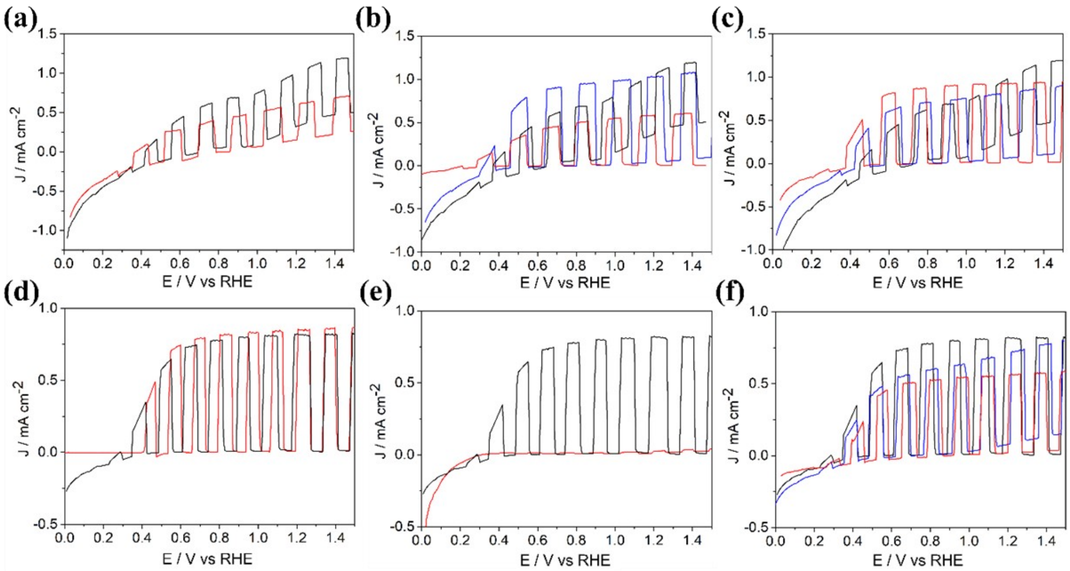

Figure S8. (a-f) Linear sweep voltammograms of TiO_2 thin films under 1 sun chopped AM 1.5 front illumination with deposition condition variations of (a) temperature: black = TiO_2-3, red = TiO_2-3-500°C, (b) deposition time: black = TiO_2-3, red = TiO_2-3-90min, blue = TiO_2-3-60min, (c) concentration: black = TiO_2-3, red = TiO_2-3-80mM, blue = TiO_2-3-120mM, (d) temperature: black = TiO_2-4, red = TiO_2-4-500°C, (e) deposition time: black = TiO_2-4, red = TiO_2-4-90min, (f) concentration: black = TiO_2-4, red = TiO_2-4-80mM, blue = TiO_2-4-120mM. All measurements performed in 1 M KOH (pH 13.7) with a 15 mV s^{-1} scan rate.

S5.3 TiO_2 Stability Measurements

Photostability measurements over a period of 3 hours were recorded using chronoamperometry (Figure S9). TiO_2-3-80 showed a greater decrease in photocurrent over the 3 hours (1.07 to 0.95 mA cm^{-2}, 11% decrease) but appeared to flatten after 150 minutes. TiO_2-4 was far less noisy, implying bubble formation had less of an impact on photocurrent, and only showed a slight decrease in performance (1.01 to 0.92 mA cm^{-2}, 8.91% decrease) with all that loss in the first 30 minutes. No significant photocurrent loss over time for both electrodes implies that no self-oxidation is taking place, and hence all photocurrent measured is due to OH^- oxidation.

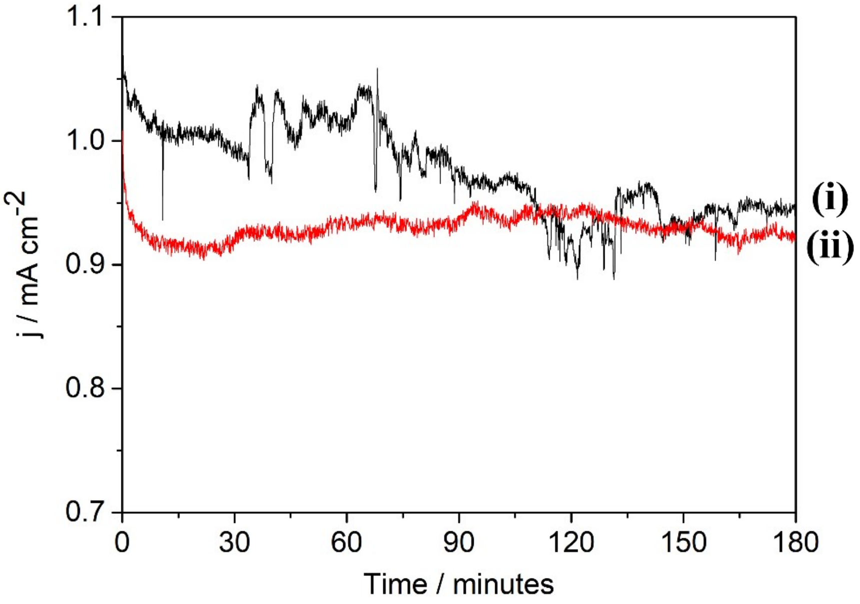

Figure S9. Photocurrent-time curves of (i) TiO_2-3-80, (ii) TiO_2-4 at an applied potential of 1.23 V vs RHE under 1 sun constant AM 1.5 illumination, performed in 1 M KOH (pH 13.7).

S6. Single-Crystal X-Ray Crystallography

S6.1 Crystal Structure

All solid-state molecular structures were determined by single crystal X-ray diffraction. The complexes are isoreticular with similar gross structural features based around the triethanolamine-metal moiety, $[Ti\{OCMe_2CH_2\}_3N]$. The molecular structures for **2**, **3** and **4** are shown in Figure S10. Structural data including important bond angles and lengths for comparison are displayed in Table S4. All structures are five-coordinate, slightly distorted trigonal bipyramids, consisting of three equatorial anionic oxygens, a transannular bridgehead nitrogen and a ligating atom in the axial plane, L, where L = NMe_2 for **2**, OEt for **3**, and OiPr for **4**, *trans* to the bridgehead nitrogen.

As shown in Table S4, the change in 'L' species from N to O is accompanied by a shortening of both the Ti-L and the transannular Ti←N bond lengths. Similar bond length contractions are also observed upon changing ancillary ligands, i.e. $\{NR_2\}$ for $\{OR\}$, for comparable monomeric Ge(IV) based systems $[(TMS_2N)Ge\{OCH_2CH_2\}_3N]$ (Ge-$NTMS_2$: 1.845 Å, Ge←N: 2.241 Å)[4] and $[(iPrO)Ge\{OCMe_2CH_2\}2\{OCH_2CH_2\}N]$ (Ge-OiPr: 1.762 Å, Ge←N: 2.180 Å).[5] While the titanium (IV) dimethylamide complex $[(Me_2N)Ti\{OCH_2CH_2\}_3N]$ is known in the literature,[6] single crystal studies reveal the molecule possesses a distorted octahedral geometry in which oxygen atoms of adjacent triethanolamine ligands bridge the titanium centres to form a molecular dimer (Ti-NMe_2: 1.944 Å, Ti←N: 2.270 Å). It is likely that the methyl groups in the triethanolamine ligand are the cause of monomer formation due to the resulting steric hindrance.

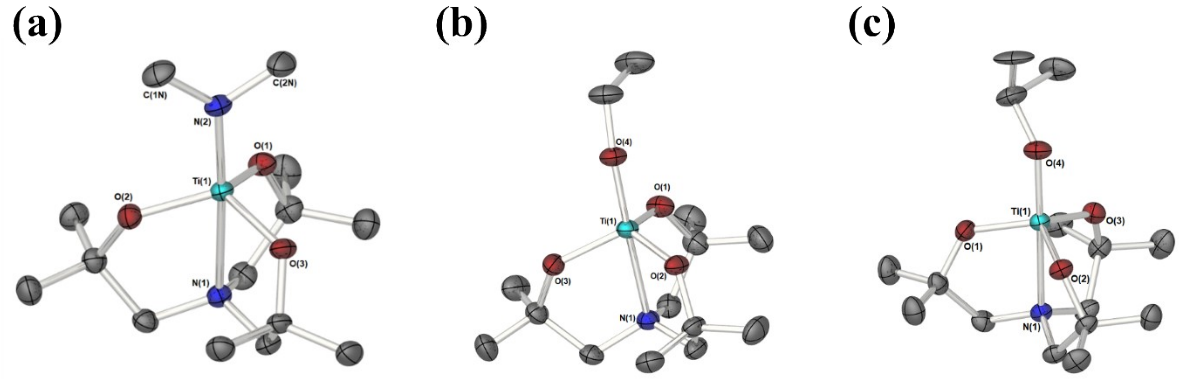

Figure S10. Molecular structures of (a) [(Me$_2$N)Ti{OCMe$_2$CH$_2$}$_3$N] (**2**), (b) [(EtO)Ti{OCMe$_2$CH$_2$}$_3$N] (**3**), (c) [(iPrO)Ti{OCMe$_2$CH$_2$}$_3$N] (**4**). H atoms omitted for clarity; thermal ellipsoids are shown at 50% probability.

The monomeric titanatrane complex **4** has previously been reported as a potential catalyst for ring opening polymerisation of cyclic esters, alongside the corresponding dimeric, and sterically less encumbered complexes [(iPrO)Ti{OCMe$_2$CH$_2$}$_2${OCH$_2$CH$_2$}N]$_2$ and [(iPrO)Ti{OCMe$_2$CH$_2$}{OCH$_2$CH$_2$}$_2$N]$_2$,[3] with identical bond lengths and angles as reported here. The thermal properties of such titanatrane, and general metallatrane, complexes have never been studied, neither their use as precursors.

Unsurprisingly, complex **3** shares very similar structural features to **4**, with Ti-O and Ti-N bond lengths and angles comparable to other monomeric 5-coordinate {TiO$_3$N} systems in the Cambridge Structural Database (CSD).[7]

Table S4. Bond lengths and angles for compounds **2**, **3**, **4**.

Compound	**2**	**3**	**4**
Ti-O	O(1): 1.8498(9)	O(1): 1.844(2)	O(1): 1.8333(11)
	O(2): 1.8195(10)	O(2): 1.843(2)	O(2): 1.8411(10)
	O(3): 1.8707(9)	O(3): 1.834(2)	O(3): 1.8400(10)
Ti-L	N(2): 1.8921(11)	O(4): 1.8098(19)	O(4): 1.8024(11)
Ti-N(1)	2.3662(11)	2.324(2)	2.3491(12)
< O-Ti-O	O(2-1): 119.53(4)	O(2-1): 116.63(9)	O(2-1): 114.65(5)
	O(2-3): 115.91(4)	O(2-3): 115.08 (10)	O(2-3): 115.12(5)
	O(1-3): 110.20(4)	O(1-3): 115.09(9)	O(1-3): 115.89(5)
$\Sigma_<$ O-Ti-O	345.64	346.8	345.66
< N-Ti-L	N(2): 176.45(5)	O(4): 177.92(9)	O(4): 176.61(5)
τ	0.95	1.02	1.012

Interestingly, complex **2** contains a relatively wide spread of bond lengths between the Ti centre atom and the equatorial oxygens. In comparison, the lengths for **3** are all within three standard deviations of each other and therefore have a >95% probability of being the same.

During our investigations, crystals of complex **5** were isolated alongside complex **3**. Single crystal X-ray diffraction experiments revealed the structure of this new complex to be a C_3-symmetric heterochiral μ-oxo dinuclear species, $[(\mu\text{-O})\{\mathrm{Ti(OCMe_2CH_2)_3N}\}_2]$, solid-state structure in Figure S11. The molecule crystallises in the monoclinic space group P2/c with half of the molecule in the asymmetric unit cell. The bridging oxygen atom is located on a crystallographic centre of inversion, such that symmetry operators generate the second half of the molecule, which results in the close to linear Ti–O–Ti bond angle (179.00474(9)°). To the best of our knowledge, this is the first reported example of an oxo-bridged metallatrane complex, however it should be noted that related tris-phenolamine supported Ti-O-Ti systems are known.[8]

The Ti–O(4) distance (1.8200(7) Å) is slightly longer than linear Ti-O-Ti-trisphenolamine systems[8] and is much closer to the range observed in similar complexes bearing a bent bridge (1.8251 and 1.8256 Å).[9] As with complexes **2**, **3** and **4** the Ti atom shows a trigonal bipyramidal geometry with Ti–N bonds of 2.40143(16) Å. Similar tripodal C_3-symmetric $\{O_3N\}$-ligand bearing complexes have attracted attention in the recent years with a wide variety of transition metals and main group elements being reported. Complete structural data including important bond angles and lengths for comparison are displayed in Table S5.

The helical conformation of the titanatrane units relative to the metal ion in **2**, **3**, and **4** are also maintained in the dimerised complex **5**. A ^{1}H NMR spectrum shows no traces of the diastereomeric homochiral complexes (Δ–Δ or Λ–Λ), meaning that a stereoselective dimerisation has occurred where only the heterochiral complex (Δ–Λ) is formed, despite the initial racemic mixture of starting material, **3**, confirmed again by ^{1}H NMR.

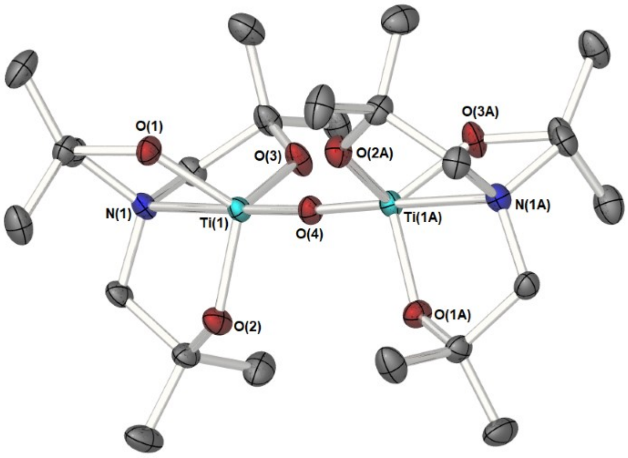

Figure S11. Molecular structure of $[(\mu\text{-O})\{\mathrm{Ti(OCMe_2CH_2)_3N}\}_2]$ (**5**). H atoms omitted for clarity; thermal ellipsoids are shown at 50% probability.

Table S5. Bond lengths and angles for compound **5**.

Compound	**5**
Ti-O	O(1): 1.827(3)
	O(2): 1.845(3)
	O(3): 1.827(3)
Ti-L	O(4): 1.8200(7)
Ti-N(1)	2.402(3)
< O-Ti-O	O(2-1): 113.90(13)
	O(2-3): 112.91(13)
	O(1-3): 116.00(13)
$\Sigma_{<}$ O-Ti-O	342.81
< N-Ti-L	O(4): 178.98(9)
τ	1.05

Top views, along the C_3 plane, can be seen in Figure S12 for the monomeric complex **3** and dimeric complex **5**. The Δ-isomer for the ligand cage around the titanium is present for **3**. The heterochiral dimer **5** is identifiable in Figure S12b, with a Λ and Δ ligand isomer on each side of the oxo-bridge.

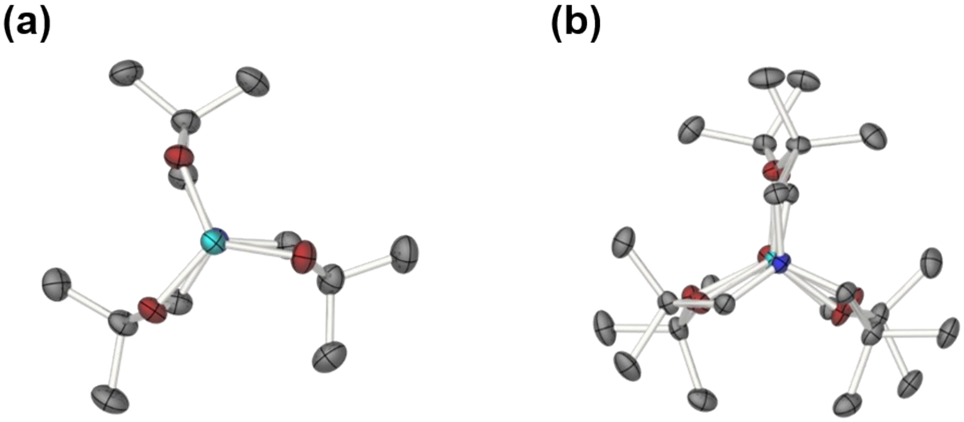

Figure S12. Top view of complexes (a) [(EtO)Ti{$OCMe_2CH_2$}$_3$N] (**3**), (b) [(μ-O){Ti($OCMe_2CH_2$)$_3$N}$_2$] (**5**), along the C_3 plane showing the 3-fold rotational symmetry. H atoms are omitted for clarity; thermal ellipsoids are shown at 50% probability.

S6.2 X-Ray Crystallography Data

Table S6. Crystal data and structure refinement for compound **2**.

Identification code	2260247	
Empirical formula	C14 H30 N2 O3 Ti	
Formula weight	322.30	
Temperature	150.01(10) K	
Wavelength	1.54184 Å	
Crystal system	Monoclinic	
Space group	$P2_1/n$	
Unit cell dimensions	a = 9.52655(8) Å	α= 90°.
	b = 27.2580(2) Å	β= 99.3958(8)°.
	c = 13.59102(12) Å	γ = 90°.
Volume	3481.90(5) Å^3	
Z	8	
Density (calculated)	1.230 Mg/m^3	
Absorption coefficient	4.236 mm^{-1}	
F(000)	1392	
Crystal size	0.394 x 0.246 x 0.134 mm^3	
Theta range for data collection	3.674 to 73.271°.	
Index ranges	-6<=h<=11, -33<=k<=33, -16<=l<=16	
Reflections collected	33405	
Independent reflections	6946 [R(int) = 0.0283]	
Completeness to theta = 67.684°	100.0 %	
Absorption correction	Gaussian	
Max. and min. transmission	1.000 and 0.402	
Refinement method	Full-matrix least-squares on F^2	
Data / restraints / parameters	6946 / 0 / 377	
Goodness-of-fit on F^2	1.034	
Final R indices [I>2sigma(I)]	R1 = 0.0285, wR2 = 0.0763	
R indices (all data)	R1 = 0.0301, wR2 = 0.0776	
Extinction coefficient	n/a	
Largest diff. peak and hole	0.322 and -0.292 e.Å^{-3}	
CCDC Number	2260244	

Table S7. Crystal data and structure refinement for compound **3**.

Identification code	2260245	
Empirical formula	C14 H29 N O4 Ti	
Formula weight	323.28	
Temperature	150.01(10) K	
Wavelength	1.54184 Å	
Crystal system	Triclinic	
Space group	P-1	
Unit cell dimensions	a = 9.4321(3) Å	α= 86.629(4)°.
	b = 9.6745(4) Å	β= 88.435(3)°.
	c = 19.0259(8) Å	γ = 80.670(3)°.
Volume	1709.92(12) Å^3	
Z	4	
Density (calculated)	1.256 Mg/m^3	
Absorption coefficient	4.343 mm^{-1}	
F(000)	696	
Crystal size	0.291 x 0.127 x 0.104 mm^3	
Theta range for data collection	4.639 to 73.252°.	
Index ranges	-11<=h<=9, -12<=k<=11, -23<=l<=23	
Reflections collected	11952	
Independent reflections	6637 [R(int) = 0.0324]	
Completeness to theta = 67.684°	99.5 %	
Absorption correction	Semi-empirical from equivalents	
Max. and min. transmission	1.00000 and 0.67937	
Refinement method	Full-matrix least-squares on F^2	
Data / restraints / parameters	6637 / 0 / 395	
Goodness-of-fit on F^2	1.080	
Final R indices [I>2sigma(I)]	R1 = 0.0497, wR2 = 0.1107	
R indices (all data)	R1 = 0.0650, wR2 = 0.1177	
Extinction coefficient	n/a	
Largest diff. peak and hole	0.406 and -0.387 e.Å^{-3}	
CCDC Number	2260245	

Table S8. Crystal data and structure refinement for compound **4**

Identification code	2260246	
Empirical formula	C15 H31 N O4 Ti	
Formula weight	337.31	
Temperature	150.00(10) K	
Wavelength	1.54184 Å	
Crystal system	Monoclinic	
Space group	$P2_1/n$	
Unit cell dimensions	a = 9.46549(10) Å	α= 90°.
	b = 13.05943(14) Å	β= 91.4818(9)°.
	c = 14.98051(15) Å	γ = 90°.
Volume	1851.18(3) Å^3	
Z	4	
Density (calculated)	1.210 Mg/m^3	
Absorption coefficient	4.032 mm^{-1}	
F(000)	728	
Crystal size	0.100 x 0.030 x 0.020 mm^3	
Theta range for data collection	4.492 to 73.191°.	
Index ranges	-11<=h<=11, -15<=k<=16, -18<=l<=12	
Reflections collected	16233	
Independent reflections	3689 [R(int) = 0.0348]	
Completeness to theta = 67.684°	99.9 %	
Absorption correction	Semi-empirical from equivalents	
Max. and min. transmission	1.00000 and 0.65041	
Refinement method	Full-matrix least-squares on F^2	
Data / restraints / parameters	3689 / 24 / 229	
Goodness-of-fit on F^2	1.035	
Final R indices [I>2sigma(I)]	R1 = 0.0317, wR2 = 0.0882	
R indices (all data)	R1 = 0.0328, wR2 = 0.0892	
Extinction coefficient	0.0040(3)	
Largest diff. peak and hole	0.266 and -0.311 e.Å^{-3}	
CCDC Number	2260246	

Table S9. Crystal data and structure refinement for compound **5**.

Identification code	2260244	
Empirical formula	C24 H48 N2 O7 Ti2	
Formula weight	572.44	
Temperature	150.01(10) K	
Wavelength	1.54184 Å	
Crystal system	Monoclinic	
Space group	P2/c	
Unit cell dimensions	a = 12.5296(6) Å	α= 90°.
	b = 9.5707(4) Å	β= 107.738(5)°.
	c = 12.5976(6) Å	γ = 90°.
Volume	1438.85(12) Å^3	
Z	2	
Density (calculated)	1.321 Mg/m^3	
Absorption coefficient	5.068 mm^{-1}	
F(000)	612	
Crystal size	0.075 x 0.030 x 0.030 mm^3	
Theta range for data collection	3.704 to 68.238°.	
Index ranges	-15<=h<=13, -10<=k<=11, -15<=l<=12	
Reflections collected	8446	
Independent reflections	2620 [R(int) = 0.0440]	
Completeness to theta = 67.684°	99.2 %	
Absorption correction	Semi-empirical from equivalents	
Max. and min. transmission	1.00000 and 0.61508	
Refinement method	Full-matrix least-squares on F^2	
Data / restraints / parameters	2620 / 0 / 165	
Goodness-of-fit on F^2	1.101	
Final R indices [I>2sigma(I)]	R1 = 0.0539, wR2 = 0.1334	
R indices (all data)	R1 = 0.0701, wR2 = 0.1406	
Extinction coefficient	n/a	
Largest diff. peak and hole	0.715 and -0.584 e.Å^{-3}	
CCDC Number	2260247	

Electronic Supplementary Information

References

1 L. J. Farrugia, *J. Appl. Crystallogr.*, 1999, **32**, 837–838.

2 O. V. Dolomanov, L. J. Bourhis, R. J. Gildea, J. A. K. Howard and H. Puschmann, *J. Appl. Crystallogr.*, 2009, **42**, 339–341.

3 S. deok Mun, S. H. Kim, J. Lee, H. J. Kim, Y. Do and Y. Kim, *Polyhedron*, 2010, **29**, 379–383.

4 S. N. Nikolaeva, K. Megges, J. Lorbeth and V. S. Petrosyan, *Z.Naturforsch., BChem. Sci.*, 1998, **53**, 973.

5 J. H. Moon, S. H. Kim, K. M. Lee, T. S. You, Y. Do and Y. Kim, *Polyhedron*, 2011, **30**, 2333–2338.

6 A. A. Naiini, W. M. P. B. Menge and J. G. Verkade, *Inorg. Chem.*, 2002, **30**, 5009–5012.

7 C. R. Groom, I. J. Bruno, M. P. Lightfoot and S. C. Ward, *Acta Cryst.*, 2016, **72**, 171–179.

8 G. Bernardinelli, T. M. Seidel, E. P. Kündig, L. J. Prins, A. Kolarovic, M. Mba, M. Pontini and G. Licini, *Dalt. Trans.*, 2007, **16**, 1573–1576.

9 V. Ugrinova, G. A. Ellis and S. N. Brown, *Chem. Commun.*, 2004, **4**, 468–469.